PCCP

Accepted Manuscript

ROYAL SOCIETY OF CHEMISTRY

www.rsc.org/pccp

Implications of boron doping on electrocatalytic activities of graphyne and graphdiyne family: A first principles study

Bikram Kumar Das[1], Dipayan Sen[1], and K. K. Chattopadhyay[1, 2, *]

1) Thin Film and NanoScience Laboratory, Department of Physics,

Jadavpur University, Kolkata 700032, India

2) School of Materials Science & Nanotechnology,

Jadavpur University, Kolkata 700032, India

*) Corresponding author; email: kkc@phys.jdvu.ac.in; Phone: +913324572876

Dispersive force corrected density functional theory is used to map the oxygen reduction reaction (ORR) kinetics of six kinds of graphyne (Gy) and graphdiyne (Gdy) systems (namely αGy, βGy, γGy, δGy, 6,6,12Gy, RGy and Gdy) with substitutional boron (B) atom doping. To this end, the most favorable sites for B doping for each structures are determined by comparing their formation energies and then the best configuration for di-oxygen (O_2) adsorption is computed by analyzing the corresponding adsorption energies. Even though oxygen adsorption is found to be energetically favorable on all of these and All the Gys and Gdy are found to distinctly favor the four electron pathways for ORR, a reaction scheme with monotonically exothermic ΔG is observed only for B doped RGy. Further computations performed by varying electrode potential indicated this monotonically exothermic nature of the ΔG of B doped R Gy to persist in the range 0 ~ 0.22 V and also indicated the first (H^+ + e) transfer step to be the rate limiting step.

Keywords: graphyne, graphdiyne, oxygen, electrocatalysis, boron

1. Introduction

Gradual depletion of stock fossil fuel reserves and ever increasing demand of "green", pollution-free energy has lately led to a global search[1,2] for clean and economic alternative energy solutions. Fuel cells, in this regard, are a developing and highly promising technology[3,4] that can directly convert chemical energy into electrical energy by mediating recombination of hydrogen and oxygen fuels into water. They offer unique multi-faceted advantages such as exceptionally high theoretical efficiency and power density coupled with zero pollution[5]; however a few key problems[6,7] still exists that are actively stifling their mainstream adoption. Slow oxygen reduction reaction (ORR) kinetics at cathode constitutes one of the major bottlenecks for the fuel cells[8] and the efficiency of cathode electrocatalyst deployed thus crucially affects their overall operating efficiency[9]. Platinum (Pt) has been the most used cathode electrocatalyst material till date[10,11]; but its vulnerability to toxicity by CO like intermediate species and sluggish ORR kinetics, along with its low abundance in nature and prohibitive cost[12-14] have manifested as niche applications to these highly promising devices rather than large scale commercialization.

Advent of two dimensional crystallites in the last decade induced a fresh spur of growth to this field as their exotic surface properties and large surface to volume ratio are highly desirable[15] for catalysis. Recent studies indicate that systems such as, nitrogen and boron doped graphene[16,17], defect graphene[18], nitrogen and boron doped carbon nanotubes[19,20], graphitic carbon nitride g-C_3N_4[21] could offer significant edge as alternate electrocatalysts over their traditional counterpart. These carbon based materials, in particular, have garnered significant research attention in the recent times due to their high surface area, excellent electrical

conductivity, low cost, high electrocatalytic activity, higher stability and durability and their highly resistive nature to CO poisoning and fuel cross-over through the membrane[22]. In this regard, various acetylene bonded 2D, all-carbon networks such as graphyne[23-25] and derived structures[26] could be speculated to provide better alternatives as they have intrinsic non-uniform charge distributions owing to the presence of acetylene bonds that readily incorporate localized surface charge densities[27]. First principle calculation confirmed the stability of graphynes and derived structures[25, 27-29]. Finite building blocks and cut outs of graphyne/ graphdiyne based structures have already been experimentally realized using various chemical methods and initial steps towards the preparation of extended structures in this regard are currently actively being pursued[30,31].

For designing ORR electrocatalysts and other electrochemical devices, conventional all-carbon networks such as pristine graphene or CNT are usually tailored with localized charge densities by the means of intrinsic (vacancy) or extrinsic (doping/ adsorption) defects so that they can facilitate better oxygen adsorption[32] and improve energy storage capacity[33,34]. In particular, previous reports[17,35] indicate that substitutional boron doping in these materials is highly advantageous for dioxygen adsorption. The difference between the electronegativity (χ) of boron (χ =2.04)[36] and carbon (χ =2.55)[37] ensures significant amount of charge transfer and the dopant boron itself, being more electropositive than carbon, acts as an active center for dioxygen adsorption. Additionally it has also been shown[32] that the dopant boron, in such cases facilitates further charge transfer to the dioxygen molecule and weakens O-O bond, thus paving the path for easier splitting of the dioxygen molecule in the subsequent reaction steps. Although, designing of ORR electrocatalysts based on graphyne and derived structures is still a very nascent field[38], similar B doping scheme could also be deployed for them. In a recent work Kong et al[39] reported

that boron doping in γGy introduced local positive charge density and local high spin density facilitated ORR in an efficient four electron process. Also in another very recent work, Chen et al[40] showed that edge terminated B doped γGy could show catalytic activity for ORR. Even though the above mentioned reports show great promise, to best of authors' knowledge, till now, no extensive investigation was carried out on ORR activities of various graphyne/graphdiyne structures and and with the current work, the authors' aim is to fill up the void.

In the present report, an exhaustive and systematic study of the electrocatalytic activities of several boron doped graphynes (αGy, βGy, γGy, δGy, 6,6,12Gy and RGy) and graphdiyne (Gdy) systems is presented. Each structure was initially doped with boron (1.3-3.1%) atoms in all possible high symmetric sites to determine the optimum doping configurations. Electronic properties of such most stable doping configurations are then explored in detail to investigate the nature of C-B interactions. The first step of ORR *i.e.* dioxygen adsorption, is carried out for each structure on every possible site linked with the boron sites. Stabilities of different adsorption sites are then compared to evaluate the most stable configuration of dioxygen adsorption on the B doped graphyne and graphdiyne structures. The subsequent steps of ORR cycle for all the concerning systems are then studied and previous reported results, where present, are critically reexamined. The effect of variation of electrode potential is also taken into account and the rate limiting step(s) of the favorable reaction pathways are isolated and identified.

2. Theoretical methods

The first-principles calculations were performed using Vienna *Ab initio* Simulation Package (VASP)[41-44] and projector-augmented-wave (PAW)[45] approach. Perdew–Burke–

Ernzerhof (PBE) functional[46] within the generalized gradient approximation (GGA) was used to compute the exchange and correlation terms. Plane wave basis up to an energy cut off 400 eV were utilized in all calculations. For geometrical optimizations, Brillouin zone integrations were carried out using **k**-points spacing of ~0.5/A^0 centered at the $\boldsymbol{\Gamma}$ point and the systems were allowed to fully relax relax until the forces were converged below 1×10^{-2} eV/ Å and the total energies were converged below 1×10^{-5} eV per atom. All pristine graphyne/ graphdiyne systems were fully (cell parameters as well as the internal atomic positions) relaxed and the thus optimized structures were used in subsequent B doping/ O_2 adsorption steps. All calculations were performed in spin unrestricted manner. Bader analysis[47] was used to calculate the charge transfer between the adatoms and hosts. Contributions of van der Waals forces were also taken into account to facilitate improved accuracy by using PBE+D2 forcefield (Grimme's) method[48] which provides one of the best balanced results.

All pristine structures were initially optimized and the computed lattice parameters are listed in table S1. A 2×2 supercell of each such structure was used for substitutional B doping studies, O_2 adsorptions and subsequent ORR kinetics calculations. Space groups, total number of atoms in the supercells and B doping percentages for different graphynes and graphdiyne structures are also listed in table S1. Notably, it was found that the lattice parameters for RGy, as reported by Yin et al.[24] do not lead to a stable structure. Present computations suggest a much lower a = b = 6.02 A^0 lattice parameter for RGy. However as other properties of RGy reported by them is fully consistent with the present results, we presume that it was a mere typographic error on the prior report. For all present calculations, a vacuum slab of length 20 Å was used in perpendicular direction to ward off the spurious interactions with its own periodic image.

To study the relative stability of the different B (boron) doping configurations, their formation energies were computed using the following relation.

$$E_{for} = E_{d\text{-}gy/gdy} - E_{gy/gdy} + n_v\mu_C - n_B\mu_B \quad (1)$$

where E_{for} is the formation energy of the doped structure, $E_{d\text{-}gy/gdy}$ and $E_{gy/gdy}$ are the total ground state energies of the doped graphyne/ graphdiyne structures and pristine graphyne/ graphdiyne structures respectively, n_v is the number of carbon atom replaced due to the course of doping, μ_C is the chemical potential of carbon atom calculated with respective graphyne/ graphdiyne system as reference state , n_B is the number of doped boron atoms and μ_B is the chemical potential of the boron atom which was calculated from rhombohedral α-boron (space group: R-3m) as reference state. Low values of formation energy, as obtained from the above, indicates better stability of the system under consideration. Dioxygen adsorption capacity of various doped Gys/ Gdy structures was derived using the following relation:

$$E^{do}_{ads} = E^{do}_{tot} - E_P - E^{do} \quad (2)$$

where, E^{do}_{ads} is the adsorption energy of dioxygen on a host, E^{do}_{tot} is the total energy of the dioxygen adsorbed host, E_P is the total energy of the host adsorbent and E^{do} is the energy of free dioxygen molecule. Lower values of adsorption energies, as obtained from the above, implies stronger adsorption.

For calculating the free energy change diagram, we assumed a low temperature acidic media based fuel cell system and calculated the free energy change for each step using the formula

$$\Delta G = \Delta E + \Delta ZPE - T\Delta S + \Delta G_U + \Delta G_{pH} \quad (3)$$

where ΔE is the change in enthalpy (here binding energy), ΔZPE is the change of zero point energy (neglected in our calculation), ΔS is the change in entropy, $\Delta G_U = -eU$ (U is the electrode

potential with respect to the standard hydrogen electrode) and ΔG_{pH} = 2.303kT pH(K Is Boltzman constant). We considered acidic medium (ideal situation of pH = 0) and T = 0K to study the ORR on different structures. The ΔE values were obtained from DFT calculation whereas the change in entropy was taken from standard table[49] for gas phase molecules to account for the change in entropy due to loss of translational degrees of freedom. The free energy of (H^+ + e) was calculated as suggested by Srinivasu et al.[50] as equal to the free energy of $1/2H_2$ at standard condition of U = 0 V and pH = 0, but equal to $1/2H_2$- eU at a finite potential U.

3. Results and Discussion

3.1. B doping in graphyne and graphdiyne

In the present work, substitutional boron doping in Gy and Gdy systems and their performances as ORR eletrocatalyst is explored by the means of first principles calculations. The Gy/ Gdy systems are selected on the basis of prior reports that established the (possible) existence of the respective phases by the means of either experimental evidence(s) or by rigorous first principles calculations (using phonon dispersions etc.). Hypothesized structures that did not meet the above criteria were not considered in the present work. The following systems were studied: αGy, βGy, γGy, δGy, 6,6,12Gy, RGy and Gdy (references to the corresponding prior works that established their phases are mentioned in table S1). The presence of both sp^2 and sp bonds in Gy/ Gdy systems implies that, for the purposes of substitutional doping, each of the surfaces contain multiple highly symmetric doping sites (in contrast to sp^2 bonded graphene, which has only one highly symmetric doping site). Supercells of all considered structures are

shown in Figure 1 (a)-(e) and Figure 2 (a)-(b), where the highly symmetric doping sites are marked by dotted overlays (black dots for sites hosting sp^2 hybridized C atoms and white dots for sites hosting sp hybridized C atoms). We adopt the following naming scheme to uniquely identify the highly symmetric sites: The first part designates the position (Ch for chain, H for hexagonal and R for rectangular/ square rings), with hybridizations (sp or sp^2) in the subscripts and (when required) relative position with respect to the rings (n for near, f for far, x for not linked to another ring) in the superscripts; and the second part designates the respective Gy/ Gdy system. To determine the most favorable B doping configuration, formation energies of B doping on each of the highly symmetric sites of each considered systems were calculated using eq (1).

αGy, βGy and γGy (Figure 1 (a)-(c)) each have only two highly symmetric doping sites, namely H_{sp2}-αGy and Ch_{sp}-αGy, H_{sp2}-βGy and Ch_{sp}-βGy and H_{sp2}-γGy and Ch_{sp}-γGy respectively with sp^2 bonded C atoms exclusively in hexagonal sites and sp bonded C atoms exclusively in chain sites. We obtained 0.71 eV and 1.87 eV, 0.19 eV and 1.46 eV, and 0.79 eV and 1.77 eV formation energies of B doping for them respectively. In all of the above three cases it can be readily observed that B dopants at hexagonal sites are by far more stable. δGy (Figure 1 (d)) has a slightly more complex configuration with chain sites having both sp and sp^2 bonded C atoms. For H_{sp2}-δGy, Ch_{sp}-δGy and Ch_{sp2}-δGy systems we obtained formation energies of 1.15 eV, 1.91 eV and 0.61 eV respectively for B doping with Ch_{sp2}-δGy being the most favorable site. Gdy (Figure 1 (e)) also have three highly symmetric doping sites, but with two sp hybridized C atoms in chain sites where one of them is closer to the hexagonal ring. In this case, for B doping in H_{sp2}-Gdy, Ch^{n}_{sp}-Gdy and Ch^{f}_{sp}-Gdy sites, we obtained formation energies of 0.62 eV, 1.45 eV and 1.51 eV respectively implying the H_{sp2}-Gdy to be the most preferable. 6,6,12Gy (Figure 2 (a)) has a complex configuration having five highly symmetric doping sites of which two are

situated in hexagonal ring corners; one of them is directly linked to a similar hexagonal ring through a acetylinic chain (H_{sp2}-6,6,12Gy) while the other is not (H^{x}_{sp2}-6,6,12Gy). They above two links also host two sp hybridized sites (Ch_{sp}-6,6,12Gy and Ch^{x}_{sp}-6,6,12Gy respectively). In addition, there is another sp2 hybridized carbon atom, but at the end of a chain (Ch_{sp2}-6,6,12Gy). The calculated formation energies for B doping in these five sites are found to be 0.37 eV, 0.61 eV, 1.48 eV, 1.49 eV and 0.21 eV respectively with B doping in Ch_{sp2}-6,6,12Gy leading to the most stable configuration. Lastly for RGy (Figure 2 (b)), there are two highly symmetric sites with sp^2 hybridized C atoms exclusively in the rectangular/square ring corner sites and the sp hybridized C atoms exclusively in the chain sites. For these R_{sp2}-RGy and Ch_{sp}-RGy sites we obtained B doping formation energies of 0.62 eV and 1.72 eV respectively; *i.e.* analogous to the cases of α/β/γ-Gys, R_{sp2}-RGy site is the more preferable site by far. Calculated values of formation energies, bond lengths of the bonds between B and nearest sp^2 and sp hybridized C atoms and charge transfer from B atom for the most stable configurations of B doping for the above seven systems are listed in Table 1. and the formation energies and charge transfer for all other considered systems are listed in Table S2. Analyzing the optimized structures and trends of formation energies, a few interesting inferences could be drawn: a) The most preferred sites of B doping are the sp^2 bonded C atom sites. b) Among two sp^2 bonded C atom sites with one C atom in a chain site and the other in a rectangular/ square/ hexagonal ring site, the most preferred site of B doping is the chain site c) All the doped graphyne and graphdiyne structures maintained their planarity after optimization.

We performed Bader charge analysis to calculate the partial charges of the atoms and charge transfers for the most favorable B doped configurations for each of the seven considered systems. We found, for H_{sp2}-αGy, H_{sp2}-βGy, H_{sp2}-γGy, Ch_{sp2}-δGy, H_{sp2}-Gdy, Ch_{sp2}-6,6,12Gy and

R_{sp2}-RGy configurations, respectively 1.98e, 1.94e, 1.92e, 1.95e, 1.92e, 1.95e and 1.87e charges transfer from the dopant B atoms to its neighboring C atoms. At a result, for all the cases, the B atoms become positively charged and its neighboring C atoms become negatively charged, rendering considerable amount of ionicity to the B-C bonds. Dopant atom charge transfers along with respective formation energies for each of the seven considered systems are shown graphically in Figure 2 (c). It was also noted, among various configurations of each systems, formation energies are correlated with the dopant atom charge transfers in a manner such that the best formation energies are always obtained for the cases where highest amount of charge transfer take place. The total and projected (onto orbitals and atoms) density of states (TDOS and PDOS of the seven considered systems are shown respectively in Figure 3 and Figure 4. TDOS plots indicate that: a) Pristine Gys and Gdy are completely non-magnetic in nature. b) B doped H_{sp2}-αGy, H_{sp2}-βGy and H_{sp2}-γGy configuration for α/ β/ γ Gys have negligible amount of spin polarizations (0.2%, 0.67%, 0.13% respectively; calculated as: $P(E_F) = (((D(E_F,\uparrow) \sim D(E_F,\downarrow)) / (D(E_F,\uparrow) + D(E_F,\downarrow))) \times 100$ where $D(E_F,\uparrow)$ and $D(E_F,\downarrow)$ values of TDOS for up and down spin electrons at the Fermi level.). c) B doped Ch_{sp2}-δGy, H_{sp2}-Gdy, Ch_{sp2}-6,6,12Gy and R_{sp2}-RGy configurations have noticeably high spin polarizations (12%, 7%, 9% and 24% respectively). From the PDOS of Ch_{sp2}-δGy (Figure 4d), it is evident that the spin polarization principally originates from the B atom's p orbital and there is a little contribution of p orbital of the C atom in the chain nearest to it. For H_{sp2}-Gdy (Figure 4e), both the dopant B atom's and its nearest C atom's (in the hexagonal ring) p orbitals contribute significantly to the spin polarization, whereas the contribution from the p orbital of the nearest C atom in the chain is negligible. For both Ch_{sp2}-6,6,12Gy (Figure 4f, 4g) and R_{sp2}-RGy, the p orbitals of the dopant B atom and its nearest C atoms (in the hexagonal ring and in the chain) contribute significantly to

the spin polarization. Notably, most of PDOS graphs show presence of various degree orbital hybridizations between the p orbitals; however for a few configurations (H_{sp2}-βGy, Ch_{sp2}-δGy) no such hybridizations can be observed. Cumulative effects of the electronic interactions for all seven considered systems are graphically visualized in Figure 5 using charge density difference diagrams along [0 0 1] direction and along the Gy/ Gdy surface using a reverse rainbow scale where electron enrichment is shown in red and electron depletion is shown in blue. Asymmetricity of the electron cloud along the B-C bonds (in contrast to symmetric electron cloud along a covalent C-C bond) which imparts iconicity to them is highlighted in Figure 5 (g). Strong bonding B and C atoms via such mixed ionic and covalent interactions readily explains the dopant B atoms' affinity towards sp^2 bonded C sites (which always have three bonds) over sp bonded C sites (which always have two bonds) as in case of the former, coordination number is always higher, which leads to better stability.

3.2. O_2 adsorption on B doped graphyne and graphdiyne

In the following section, as a perquisite for studying the ORR kinetics in Gy/ Gdy systems, the adsorption of dioxygen molecule (O_2) on them is investigated. For O_2 adsorption, only side-on modes[51] and along the bridge orientations[52] are taken into account as according to previous reports[51-52] on similar systems, significantly better adsorption energies were observed when both O atoms interacted with the substrate. As the dopant B sites are positively charged (due to their being less electronegative than surrounding C atoms), they effectively act as an active anchor for O_2 molecules and facilitate better adsorption[39]. We have systematically explored O_2 adsorption on all possible B doped Gy/ Gdy configurations and observed O_2 to

adsorb most strongly when the B atom was doped in sp bonded C atom sites (*i.e.* in $Ch^{<n/f//x>}_{sp}$-Gy/Gdy configurations). However, in most of those cases the interactions were so strong that the substrates were oxidized, resulting in complete breaking down of molecular O_2 and thus constituting a bottleneck for ORR. Coupled with our observation the $Ch^{<n/f//x>}_{sp}$-Gy/Gdy universally has worse stability than $H/Ch/R^{<n/f//x>}_{sp2}$-Gy/Gdy configurations, we will focus the rest of the discussion on $H/Ch/R^{<n/f//x>}_{sp2}$-Gy/Gdy and specifically on the most favorable B doped configurations of each Gy/ Gdy systems. For each such system, all possible O_2 adsorption configurations were studied and the most favorable adsorption configuration was identified by calculating adsorption energies using eq (2).

To study O_2 adsorption, the following configurations were studied: a) for H_{sp2}-αGy, along the B-C_{sp} bridge, b) for H_{sp2}-βGy, along the B-C_{sp2} and B-C_{sp} bridges, c) for H_{sp2}-γGy, along the B-C_{sp2} and B-C_{sp} bridges, d) for Ch_{sp2}-δGy, along the B-C_{sp} bridge e) for H_{sp2}-Gdy, along the B-C_{sp2} and B-C_{sp} bridges f) for Ch_{sp2}-6.6.12Gy, along the B-C_{sp2} and B-C_{sp} bridges and g) for R-S_{sp2}Gy, along the B-C_{sp2} and B-C_{sp} bridges. The most favorable adsorption geometries among the above are shown in Figure 6 (a)-(g) respectively and we obtained adsorption energies of -0.21 eV, -0.29 eV, -0.04 eV, -0.06 eV, -0.24 eV, -0.16 eV and -0.81 eV for them respectively; *i.e.* for all these seven configurations spontaneous O_2 adsorptions are possible. Strong interactions in these cases mostly originated from ionic bonding between B and O atoms and C-p and O-p state hybridizations (for more detailed analysis see supporting information (Figure S1). It was also observed that, for these cases, certain amount of charge transfer (0.96e - 1.05e) to the dioxygen molecule resulted in weakening of the O-O bonds and they were stretched by (17.31%-18.6%) after being adsorbed on the B doped Gy/ Gdy hosts. The values of adsorption energy, stretched bond length of O_2 molecule in adsorbed state, bond stretching percentage, distance of individual

O atom from the Gy/ Gdy plane and total charge transfer to the O_2 molecule of the most favorable configurations of O_2 adsorption on the above seven systems are listed in Table 2 and the same for all other possible configurations are listed in Table S2. From the above data, it can be inferred that all these seven systems show requisite characteristics for ORR electrocatalysis as they facilitate strong adsorption of molecular dioxygen without oxidizing the surface and they weaken the O-O bond sufficiently so that subsequent hydrogenations can take place. The actual performance of them in an ORR cycle will be discussed in the following section.

3.3. Oxygen reduction reaction kinetics

In the following section, activities of the all the seven B doped Gy and Gdy configurations (*i.e.* H_{sp2}-αGy, H_{sp2}-βGy, H_{sp2}-γGy, Ch_{sp2}-δGy, H_{sp2}-Gdy, Ch_{sp2}-6,6,12Gy and R_{sp2}-RGy) as prototype cathode electrocatalysts of a low temperature acidic media based fuel cell are systematically explored. In the current context, dioxygen molecule can be reduced via two distinct pathways: namely the two electron pathway (end product H_2O_2) and the four electron pathway (end product H_2O). Prior reports[16] suggest the four electron pathway to be more efficient and thus highly desired for applied point of view. The reaction coordinates for these two processes are as follows:

Two electron pathway: (1) $O_2 + 2(H^+ + e^-) \rightarrow$ (2) $*O_2 + 2(H^+ + e^-) \rightarrow$ (3) $*OOH + (H^+ + e^-) \rightarrow$ (4) H_2O_2; in summary: $O_2 + 2(H^+ + e^-) \rightarrow H_2O_2$

Four electron pathway (can continue in two possible paths depending on whether H_2O_2 intermediate forms in the reaction or not and they are denoted here by a. and b. respectively): (1) $O_2 + 4(H^+ + e^-) \rightarrow$ (2) $*O_2 + 4(H^+ + e^-) \rightarrow$ (3) $*OOH + 3(H^+ + e^-) \rightarrow$ (4a.) $2*OH + 2(H^+ + e^-)$

or (4b.) *O + H_2O + 2(H^++ e^-) → (5) *OH + H_2O + (H^++ e^-) → (6) $2H_2O$; in summary : O_2 + $4(H^+ + e^-) \rightarrow 2H_2O$

Where * denotes a chemisorption site on catalyst. For each of the seven configurations, reaction kinetics was studied using both pathways. To evaluate electrocatalytic performances, changes of free energy (ΔG) was calculated using eq. 3 and free energy water molecules in gas phase as reference for each steps of the protonation process for each of the seven B doped Gy/Gdy configurations. In this process, we followed the suggestion put forward by Nørskov et al.[49] that during the reaction $H^+ + e^- = 1/2H_2$, both the reactant and product remain in equilibrium. The value of TS for each step was taken from a standard physical chemistry table[49] assuming the H_2 and O_2 gases are at room temperature and ambient pressure. Entropies of the adsorbed molecules were considered as negligible while comparing to the entropies of the molecules in the gas phases.

Variation of ΔG with reaction coordinates for all possible reaction paths are shown in Figure 7 and 8 (electrode potential variation). In first reaction coordinate, the O_2 molecule is lying outside of the interaction range of the catalytic surfaces and the four H^+ ions flow through the electrolyte and the four electrons flow through the outer circuit. ΔG_1 (ΔG for the reaction coordinate) is calculated to be 4.932 eV for all systems/ pathways. In the second reaction coordinate, the O_2 molecule is adsorbed on the catalytic surface and, as discussed in the previous section, is activated and primed for reduction due to lowering of O-O bond breakage barrier. ΔG_2 for R_{sp2}-RGy is calculated to be 4.761 eV, whereas the same for all others are found to be in the range 5.231 eV- 5.530 eV. The above indicates that, except for R_{sp2}-RGy all other configurations have a small free energy barrier in the second reaction coordinate *i.e.* for them this reaction step is endothermic. Though, as seen in the previous section, O_2 adsorption is spontaneous in terms of

adsorption energy, there is a small free energy barrier is present for all the configurations, except R_{sp2}-RGy when the adsorption process is analyzed in terms of free energy. However as these free energy barriers are not very much high and can be overcome by external energy easily, we proceed with all the configurations to study the subsequent ORR steps. Previously Kong et al.[39] studied ORR on edge terminated B doped γGy and Chen et al.[40] reported ORR on edge terminated B doped αGy and γGy systems, but it is to be noted that they did not include the dioxygen adsorption step (second reaction coordinate) in their reaction kinetics.

In the next step, *i.e.* the first protonation process (reaction coordinate 3), atomic H can get attached to either of the O atoms (henceforth O atom on B is denoted as O_B and the O atom on C is denoted as O_C) of the adsorbed O_2 molecule and either $*O_C$-O_BH (pathway (i) as shown in Figure 7) or $*O_B$-O_CH (pathway (ii) as shown in Figure 7) could be formed. The possibilities of formation of both were considered and if their ΔG_3 values were very close (~ 0.3 eV or less), both of them were considered for subsequent ORR steps. It was found that all the seven configurations prefers to form $*O_B$-O_CH with ΔG_3 ranging between 2.561 eV to 4.801 eV. However, it was observed that, except H_{sp2}-γGy and Ch_{sp2}-6,6,12Gy all other configurations could also form $*O_C$-O_BH due closely lying ΔG_3 values of both paths. For H_{sp2}-γGy and Ch_{sp2}-6,6,12Gy, ΔG_3 of $*O_C$-O_BH intermediates were calculated to be 5.318 eV and 4.960 eV respectively whereas, ΔG_3 of $*O_B$-O_CH intermediates were much lower, 4.606 eV and 2.561 eV (lowest ΔG_3 for all the configuration) respectively. Hence for these two systems, only $*O_B$-O_CH forming intermediate steps were considered in further studies.

The following step, *i.e.* the second protonation process (reaction coordinate 4) is critical, as it decides whether the two or four electron process will dominate. This step can proceed in two possible ways (4a. or 4b.): the 2nd H atom could either get attached to the O atom which was

unused in the first protonation process and could form 2*OH (4 a.) or it could get attached to the O which is already in the *OH state and release one water molecule with *O remaining (4 b.). Our calculations reveals that, all $*O_B$-O_CH intermediates prefer the 4b. route with significantly lower ΔG_4 values. On the other hand, except H_{sp2}-βGy, all other four configurations with $*O_C$-O_BH intermediates are found to prefer the 4a. pathway and form 2*OH. $*O_C$-O_BH formation for H_{sp2}-βGy is observed to follow the 4b. pathway and form very stable $*O_{BC}$ with ΔG_4= 1.417 eV creating another larger drop in the ΔG_4. The following points are to be noted: 1. for the configurations that preferred 4a. type path, the 2*OH was found to be anchored to the catalytic surface indicating further reduction is preferable. 2. In the cases where *O was formed, the atomic O got almost incorporated in the Gy/ Gdy plane and bonded strongly with both B and nearest C atom ($*O_{BC}$). The above observations collectively implies that for these systems, four electron ORR (both via intermediate H_2O_2 formation and not) dominates over two electron ORR.

In the 3rd protonation process (reaction coordinate 5) all the $*O_{BC}$ structures transformed into $*O_{BC}$H with the exception of H_{sp2}-Gdy which preferred $*O_B$H configuration. It was also observed that, except H_{sp2}-Gdy, all of them has higher ΔG_5 than ΔG_4, indicating endothermic trend of this step for them. On the other hand the 2*OH structures for H_{sp2}-αGy, Ch_{sp2}-δGy, H_{sp2}-Gdy and R_{sp2}-RGy configurations were observed to exothermically transform into *OH, ejecting the first water molecule in the 3rd protonation step with ΔG_5 ranging from 0.942 eV to 1.399 eV. Our obtained results for B doped γGy for this step do not agree with previous reports[37,38] where monotonic decrease of relative energies were reported. This discrepancy could be explained by the fact that a) none of these previous reports considered the entropy-temperature terms in their calculations (which introduced an error in their calculated reaction kinetics[53]) and b) they

considered an edge terminated γGy model which is grossly different from the present periodic models.

To summarize, only for R_{sp2}-RGy configuration a monotonically exothermic ORR pathway could be obtained. All other configurations, irrespective of whether H_2O_2 intermediates form or not, display an endothermic trend either/both in 2nd or/and 5th reaction coordinates. Boron doped H_{sp2}-αGy, Ch_{sp2}-δGy and H_{sp2}-Gdy configurations have exothermic trends following 2nd reaction coordinate, however their 2nd reaction coordinate itself have 0.427, 0.584 and 0.399 eV free energy barriers respectively. To gain more insight regarding ORR using R_{sp2}-RGy system, we took the effect of electrode potential (U) into account and reexamined the ORR pathway by varying electrode potential from 1.23 V to 0.2 V .The calculated ΔG vs. reaction coordinate plots at different electrode potentials are shown in Figure 8. Our calculations show that, at standard electrode potential 1.23 V, first, second and third protonation steps have uplifts. Gradual lowering the electrode potential revealed that, from 0.22 V and below, all the ORR steps become downwards. So it can be concluded that the minimum absolute overpotential for this reaction is 1.01 V. From Figure 8 it can readily inferred that, the first protonation step is the last to turn upward while decreasing the electrode potentials, thus it constitutes the rate limiting step for this ORR pathway.

4. Conclusion

In summary, in the present work, dispersive force corrected density functional theory is used to perform a systematic and exhaustive study on: a) Determining the most favorable configuration of substitutional B doping scheme on six different graphyne (Gy) structures and

graphdiyne (Gdy). b) Studying electronic properties of B doped Gy/ Gdy systems. c) Determining the most favorable adsorption configuration of O_2 on B doped Gy/ Gdy. d) Calculating the probable ORR pathways for all relevant systems.

For B doping in Gy/ Gdy, the sp^2 hybridized C atom sites are found to be more favorable than sp hybridized C atom sites as the former offers higher coordination number for bonding and thus facilitates better stability. We obtained favorable formation energies of 0.186 eV - 0.707 eV for B doping in these systems and observed the dopant atom charge transfer to be highest for energetically most favorable systems. Dioxygen adsorption energies of the (most favorable) B doped Gy/ Gdy systems ranged from -0.042 eV (for γGy) to -0.81 eV (for RGy) indicating strong and spontaneous adsorption. On each of the B doped Gy/ Gdy structure, weakening of the O-O was observed with bond stretching percentage varying from 17.31% to 18.6%.

In the next phase, all possible reaction pathways for oxygen reduction on the above mentioned B doped Gy/ Gdy systems were systematically explored. Even though all the systems were found to favor four electron pathways for ORR; except R-Gy, all of them displayed a free energy barrier in the O_2 adsorption reaction coordinate which implied these steps to be endothermic in nature. Except β-Gy (which always formed a highly stable structure and presented considerable free energy barriers) each of these systems demonstrated a common trend of forming highly stable configurations after second (H^+ + e) transfer if the first H bonded to O_C. In this case, the other O atom bonded strongly with both B and nearest C atom and got nearly incorporated in the Gy/ Gdy layer which ultimately resulted in a free energy barrier for the third (H^+ + e) transfer reaction coordinate. However, if the first H bonded to the O_B, then the remaining reaction steps became exothermic and the reaction could proceed spontaneously. Only in case of B doped R-Gy, when the first H atom bonded to O_B, a monotonically exothermic

reaction pathway could be located for the whole reaction pathway and thus this system is found to hold promise for ORR applications. Further extensive computations regarding this system were performed by varying electrode potentials starting from 1.23 V (equilibrium potential) in which all reaction steps became exothermic in the range 0 ~ 0.22 V and the first (H^+ + e) transfer step was identified to be the rate limiting step as it was the last step to become exothermic.

Acknowledgments

Two of us (BKD and DS) wish to thank the Department of Science & Technology, Govt. of India and W.B. State Govt. for providing financial support during the execution of this work. The authors also wish to thank the University grants Commission, the Govt. of India for financial support under the 'University with potential for excellence (UPE-II)' scheme and also from TEQIP programme.

References

1. C. Y. Su, B. H. Liu, T. J. Lin, Y. M. Chi, C. C. Kei, K. W. Wang and T. P. Perng, *Journal of Materials Chemistry A*, 2015, DOI: 10.1039/C5TA04383B.
2. C. Galeano, C. Baldizzone, H. Bongard, B. Spliethoff, C. Weidenthaler, J. C. Meier, K. J. Mayrhofer and F. Schüth, *Advanced Functional Materials*, 2014, **24**, 220-232.
3. W.-W. Li, H.-Q. Yu and Z. He, *Energy & Environmental Science*, 2014, **7**, 911-924.
4. L. Carrette, K. Friedrich and U. Stimming, *Fuel cells*, 2001, **1**, 5-39.
5. S. G. Peera, A. Sahu, S. Bhat and S. Lee, *RSC Advances*, 2014, **4**, 11080-11088.
6. Z. Zhang, J. Liu, J. Gu, L. Su and L. Cheng, *Energy & Environmental Science*, 2014, **7**, 2535-2558.
7. P. Ramaswamy, N. E. Wong and G. K. Shimizu, *Chemical Society Reviews*, 2014, **43**, 5913-5932.

8. P. Zhang, F. Sun, Z. Xiang, Z. Shen, J. Yun and D. Cao, *Energy & Environmental Science*, 2014, **7**, 442-450.
9. G. Zhang, B. Y. Xia and X. Wang, *Advanced Materials*, 2014, **26**, 2408-2412.
10. A. Morozan, B. Jousselme and S. Palacin, *Energy & Environmental Science*, 2011, **4**, 1238-1254.
11. R.-Q. Zhang, T.-H. Lee, B.-D. Yu, C. Stampfl and A. Soon, *Physical Chemistry Chemical Physics*, 2012, **14**, 16552-16557.
12. N. Daems, X. Sheng, I. F. Vankelecom and P. P. Pescarmona, *Journal of Materials Chemistry A*, 2014, **2**, 4085-4110.
13. C.-H. Chen, K. E. Meadows, A. Cuharuc, S. C. Lai and P. R. Unwin, *Physical Chemistry Chemical Physics*, 2014, **16**, 18545-18552.
14. P. Divya and S. Ramaprabhu, *Journal of Materials Chemistry A*, 2014, **2**, 4912-4918.
15. Y. Xue, D. Yu, L. Dai, R. Wang, D. Li, A. Roy, F. Lu, H. Chen, Y. Liu and J. Qu, *Physical Chemistry Chemical Physics*, 2013, **15**, 12220-12226.
16. L. Zhang and Z. Xia, *The Journal of Physical Chemistry C*, 2011, **115**, 11170-11176.
17. Z.-H. Sheng, H.-L. Gao, W.-J. Bao, F.-B. Wang and X.-H. Xia, *Journal of Materials Chemistry*, 2012, **22**, 390-395.
18. D. Sen, R. Thapa and K. K. Chattopadhyay, *ChemPhysChem*, 2014, **15**, 2542-2549.
19. W. J. Lee, U. N. Maiti, J. M. Lee, J. Lim, T. H. Han and S. O. Kim, *Chemical Communications*, 2014, **50**, 6818-6830.
20. L. Yang, S. Jiang, Y. Zhao, L. Zhu, S. Chen, X. Wang, Q. Wu, J. Ma, Y. Ma and Z. Hu, *Angewandte Chemie*, 2011, **123**, 7270-7273.
21. Y. Zheng, J. Liu, J. Liang, M. Jaroniec and S. Z. Qiao, *Energy & Environmental Science*, 2012, **5**, 6717-6731.
22. C. He, J. J. Zhang and P. K. Shen, *Journal of Materials Chemistry A*, 2014, **2**, 3231-3236.
23. R. Baughman, H. Eckhardt and M. Kertesz, *The Journal of chemical physics*, 1987, **87**, 6687-6699.
24. W.-J. Yin, Y.-E. Xie, L.-M. Liu, R.-Z. Wang, X.-L. Wei, L. Lau, J.-X. Zhong and Y.-P. Chen, *Journal of Materials Chemistry A*, 2013, **1**, 5341-5346.
25. M. Zhao, W. Dong and A. Wang, *Scientific reports*, 2013, **3**.

26. M. M. Haley, S. C. Brand and J. J. Pak, *Angewandte Chemie International Edition in English*, 1997, **36**, 836-838.
27. B. G. Kim and H. J. Choi, *Physical Review B*, 2012, **86**, 115435.
28. Q. Zheng, G. Luo, Q. Liu, R. Quhe, J. Zheng, K. Tang, Z. Gao, S. Nagase and J. Lu, *Nanoscale*, 2012, **4**, 3990-3996.
29. N. K. Perkgöz and C. Sevik, *Nanotechnology*, 2014, **25**, 185701.
30. J. M. Kehoe, J. H. Kiley, J. J. English, C. A. Johnson, R. C. Petersen and M. M. Haley, *Organic letters*, 2000, **2**, 969-972.
31. G. Li, Y. Li, H. Liu, Y. Guo, Y. Li and D. Zhu, *Chemical Communications*, 2010, **46**, 3256-3258.
32. X. Fan, W. Zheng and J.-L. Kuo, *Rsc Advances*, 2013, **3**, 5498-5505.
33. Y. Liu, V. I. Artyukhov, M. Liu, A. R. Harutyunyan and B. I. Yakobson, *The Journal of Physical Chemistry Letters*, 2013, **4**, 1737-1742.
34. C. Ling and F. Mizuno, *Physical Chemistry Chemical Physics*, 2014, **16**, 10419-10424.
35. L. Ferrighi, M. Datteo and C. Di Valentin, *The Journal of Physical Chemistry C*, 2013, **118**, 223-230.
36. G. R. Owen, *Chemical Society Reviews*, 2012, **41**, 3535-3546.
37. I. Y. Jeon, S. Zhang, L. Zhang, H. J. Choi, J. M. Seo, Z. Xia, L. Dai and J. B. Baek, *Advanced Materials*, 2013, **25**, 6138-6145.
38. P. Wu, P. Du, H. Zhang and C. Cai, *The Journal of Physical Chemistry C*, 2012, **116**, 20472-20479.
39. X.-k. Kong, Q.-w. Chen and Z. Sun, *RSC Advances*, 2013, **3**, 4074-4080.
40. X. Chen, Q. Qiao, L. An and D. Xia, *The Journal of Physical Chemistry C*, 2015.
41. G. Kresse and J. Hafner, *Physical Review B*, 1993, **47**, 558.
42. G. Kresse and J. Hafner, *Physical Review B*, 1994, **49**, 14251.
43. G. Kresse and J. Furthmüller, *Computational Materials Science*, 1996, **6**, 15-50.
44. G. Kresse and J. Furthmüller, *Physical Review B*, 1996, **54**, 11169.
45. P. E. Blöchl, *Physical Review B*, 1994, **50**, 17953.
46. J. P. Perdew, K. Burke and M. Ernzerhof, *Physical review letters*, 1996, **77**, 3865.
47. R. F. Bader, *Chemical Reviews*, 1991, **91**, 893-928.
48. S. Grimme, *Journal of computational chemistry*, 2006, **27**, 1787-1799.

49. J. K. Nørskov, J. Rossmeisl, A. Logadottir, L. Lindqvist, J. R. Kitchin, T. Bligaard and H. Jónsson, *The Journal of Physical Chemistry B*, 2004, **108**, 17886-17892.
50. K. Srinivasu and S. K. Ghosh, *The Journal of Physical Chemistry C*, 2013, **117**, 26021-26028.
51. H. Kim, K. Lee, S. I. Woo and Y. Jung, *Physical Chemistry Chemical Physics*, 2011, **13**, 17505-17510.
52. H. Yan, B. Xu, S. Shi and C. Ouyang, *Journal of Applied Physics*, 2012, **112**, 104316.
53. A. B. Anderson, *Electrochimica acta*, 2003, **48**, 3743-3749.

Figure caption

Figure 1. representation of highly symmetric doping sites for (a) αGy, (b) βGy, (c) γGy, (d) δGy and (e) Gdy; black circles represents sp^2 hybridized C atoms, white circles represent sp hybridized C atoms; (a)1: H_{sp2}-αGy, (a)2: Ch_{sp}-αGy; (b)1: H_{sp2}-βGy, (b)2: Ch_{sp}-βGy; (c)1: H_{sp2}-γGy, (c)2: Ch_{sp}-γGy; (d)1: H_{sp2}-δGy, (d)2: Ch_{sp}-δGy, (d)3: Ch_{sp2}-δGy; (e)1: H_{sp2}-Gdy, (e)2: Ch^{n}_{sp}-Gdy, (e)3: Ch^{f}_{sp}-Gdy.

Figure 2. representation of highly symmetric doping sites for (a) 6,6,12Gy, (b) RGy; black circles represents sp^2 hybridized C atoms, white circles represent sp hybridized C atoms; (a)1: H_{sp2}-6,6,12Gy, (a)2: H^{x}_{sp2}-6,6,12Gy, (a)3: Ch^{x}_{sp}-6,6,12Gy, (a)4: Ch_{sp2}-6,6,12Gy, (a)5: Ch_{sp}-6,6,12Gy, (b)1: R_{sp2}-RGy, (b)2: Ch_{sp}-RGy; (c) represents Formation energy and charge transfer for (a) H_{sp2}-αGy, (b) H_{sp2}-βGy, (c) H_{sp2}-γGy, (d) Ch_{sp2}-δGy, (e) H_{sp2}-Gdy, (f) Ch_{sp2}-6,6,12Gy and (g) R_{sp2}-RGy configurations.

Figure 3. Total density of states (TDOS) B doped (a) H_{sp2}-αGy, (b) H_{sp2}-βGy, (c) H_{sp2}-γGy, (d) Ch_{sp2}-δGy, (e) H_{sp2}-Gdy, (f) Ch_{sp2}-6,6,12Gy and (g) R_{sp2}-RGy configurations.

Figure 4. Partial density of states (PDOS) of B doped (a) H_{sp2}-αGy, (b) H_{sp2}-βGy, (c) H_{sp2}-γGy, (d) Ch_{sp2}-δGy, (e) H_{sp2}-Gdy, (f) Ch_{sp2}-6,6,12Gy and (g) R_{sp2}-RGy configurations. Violet (shaded), red and orange colored lines represent PDOS of B-p states, nearest sp^2 C-p states and nearest sp C-p states respectively.

Figure 5. Top view of charge density difference for B doped (a) H_{sp2}-αGy, (b) H_{sp2}-βGy, (c) H_{sp2}-γGy, (d) Ch_{sp2}-δGy, (e) H_{sp2}-Gdy, (f) Ch_{sp2}-6,6,12Gy and (g) R_{sp2}-RGy configurations. The reverse rainbow scale is shown on the right where scale values varies from -0.08(maximum electron depletion) to 0.08(maximum electron enrichment).

Figure 6. Optimized configuration for best dioxygen adsorption on B doped (a) H_{sp2}-αGy, (b) H_{sp2}-βGy, (c) H_{sp2}-γGy, (d) Ch_{sp2}-δGy, (e) H_{sp2}-Gdy, (f) Ch_{sp2}-6,6,12Gy and (g) R_{sp2}-RGy configurations (for better view the size of the oxygen atoms are made smaller than the atoms of host).

Figure 7. free energy diagrams for Oxygen Reduction Reaction on (a) H_{sp2}-αGy, (b) H_{sp2}-βGy, (c) H_{sp2}-γGy, (d) Ch_{sp2}-δGy, (e) H_{sp2}-Gdy, (f) Ch_{sp2}-6,6,12Gy and (g) R_{sp2}-RGy; (i) and (ii) denotes whether $*O_C$-O_BH or $*O_B$-O_CH is formed after the first protonation process; Reaction

coordinate: (1) O_2 + 4(H^++ e^-), (2) *O_2 + 4(H^++ e^-), (3) *OOH + 3(H^++ e^-), (4) 2*OH + 2(H^++ e^-) or *O + H_2O + 2(H^++ e^-), (5) *OH + H_2O + (H^++ e^-) and (6) 2H_2O

Figure 8. free energy diagram for oxygen reduction reaction on B doped R_{sp2}-RGy configuration at different electrode potential(U).Reaction coordinate: (1) O_2 + 4(H^++ e^-), (2) *O_2 + 4(H^++ e^-), (3) *OOH + 3(H^++ e^-), (4) 2*OH + 2(H^++ e^-), (5) *OH + H_2O + (H^++ e^-) and (6) 2H_2O

Table 1. Parameters of single B doping in pristine Gy/ Gdy systems: E_{for} is the formation energy of the B doped configurations, $d_{B\text{-}C(sp2)}$ and $d_{B\text{-}C(sp)}$ are optimized bond lengths between B and nearest sp^2 hybridized C atom and between B and nearest sp hybridized C atom respectively, Q_B is the Bader charge transfer from dopant B atom.

B doped configuration	E_{for} (eV)	$d_{B\text{-}C(sp2)}$ (A^0)	$d_{B\text{-}C(sp)}$ (A^0)	Q_B (e)
H_{sp2}-αGy	0.707	-	1.492	1.98
H_{sp2}-βGy	0.186	1.556	1.499	1.94
H_{sp2}-γGy	0.795	1.505	1.47	1.92
Ch_{sp2}-δGy	0.602	-	1.482	1.95
H_{sp2}-Gdy	0.618	1.533	1.491	1.92
Ch_{sp2}-6,6,12Gy	0.211	1.546	1.483	1.95
R_{sp2}-RGy	0.644	1.546	1.447	1.87

Table 2. Parameters for O_2 adsorption on B doped Gy/ Gdy hosts: E^{do}_{ads} is the O_2 adsorption energy, $d_{O\text{-}O}$ is the bond length of O_2 in adsorbed state, $\Delta d_{O\text{-}O}$ is the amount of stretching occurred after adsorption, $d_{O(B)\text{-}Gy/\ Gdy}$ is the distance of the O atom adsorbed on B from the Gy/ Gdy plane, $d_{O(C)\text{-}Gy/\ Gdy}$ is the distance of O atom adsorbed on C from the Gy/ Gdy plane, Q_O is the bader charge transferred to the O_2 molecule during adsorption.

Configuration	O_2 adsorption site	E^{do}_{ads} (eV)	$d_{O\text{-}O}$ (A^0)	$\Delta d_{O\text{-}O}$ (%)	$d_{O(B)\text{-}Gy/\ Gdy}$ (A^0)	$d_{O(C)\text{-}Gy/\ Gdy}$ (A^0)	Q_O (e)
H_{sp2}-αGy	B-C_{sp} bridge	-0.213	1.471	18.44	1.557	1.388	1.04
H_{sp2}-βGy	B-C_{sp} bridge	-0.289	1.468	18.2	1.554	1.409	1.03
H_{sp2}-γGy	B-C_{sp2} bridge	-0.042	1.457	17.31	1.541	1.497	0.96
Ch_{sp2}-δGy	B-C_{sp} bridge	-0.056	1.467	18.12	1.562	1.387	0.99
H_{sp2}-Gdy	B-C_{sp} bridge	-0.241	1.466	18.03	1.567	1.393	1.02
Ch_{sp2}-6,6,12Gy	B-C_{sp} bridge	-0.161	1.473	18.6	1.552	1.399	1.05
R_{sp2}-RGy	B-C_{sp} bridge	-0.81	1.468	18.2	1.527	1.408	1.03

Figure 1.

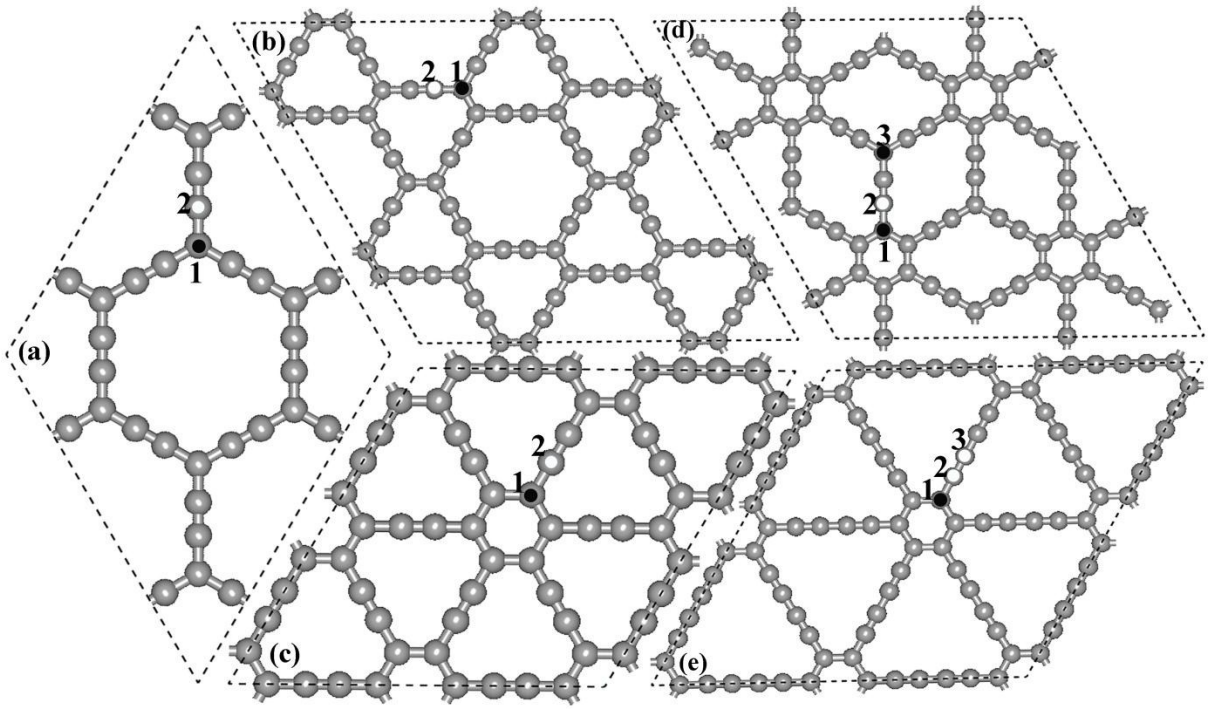

Figure 2.

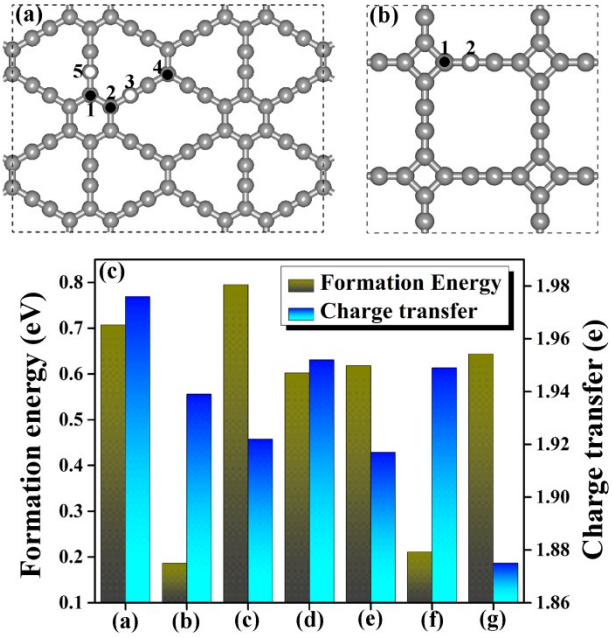

Figure 3.

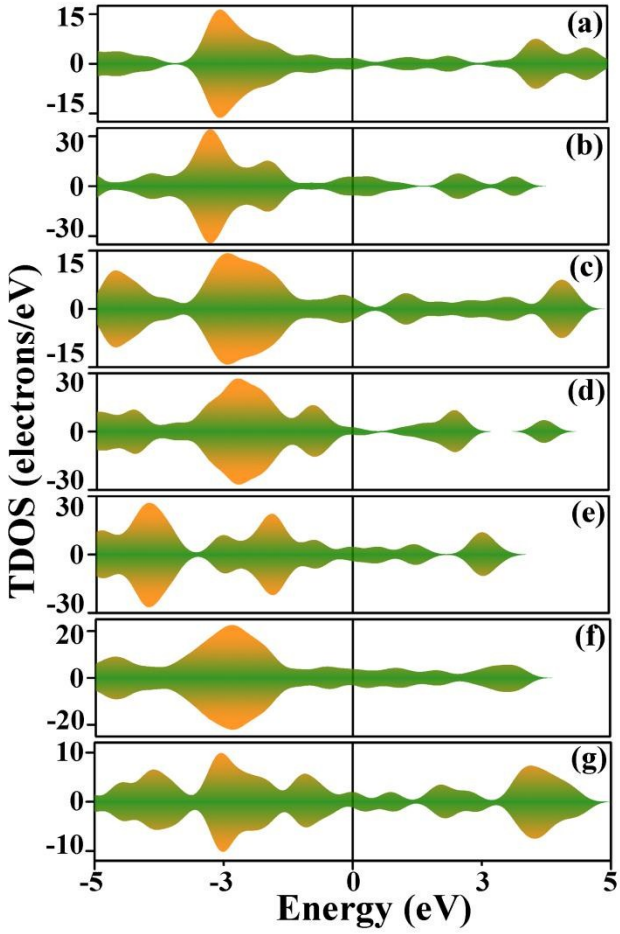

Figure 4.

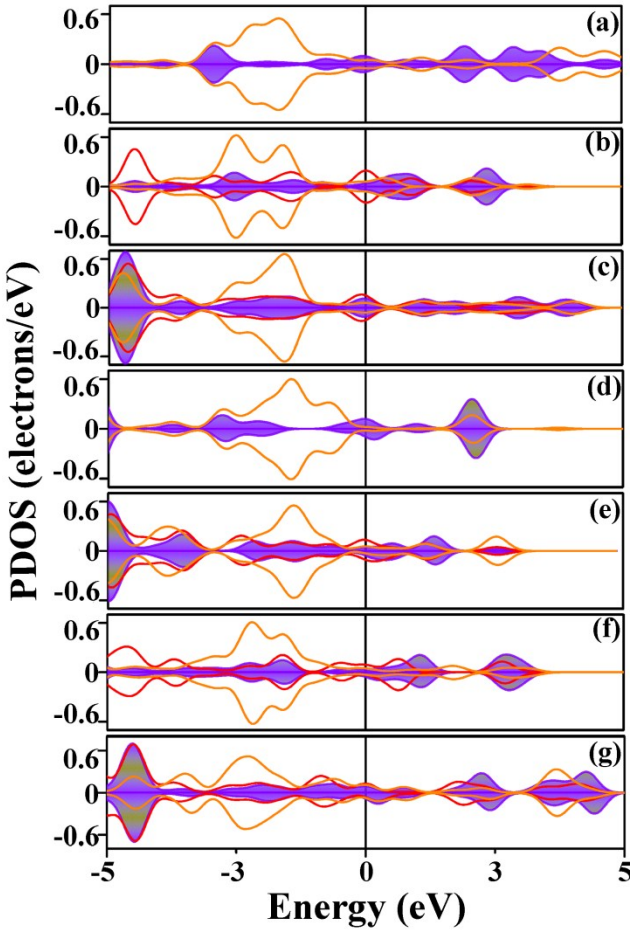

Figure 5.

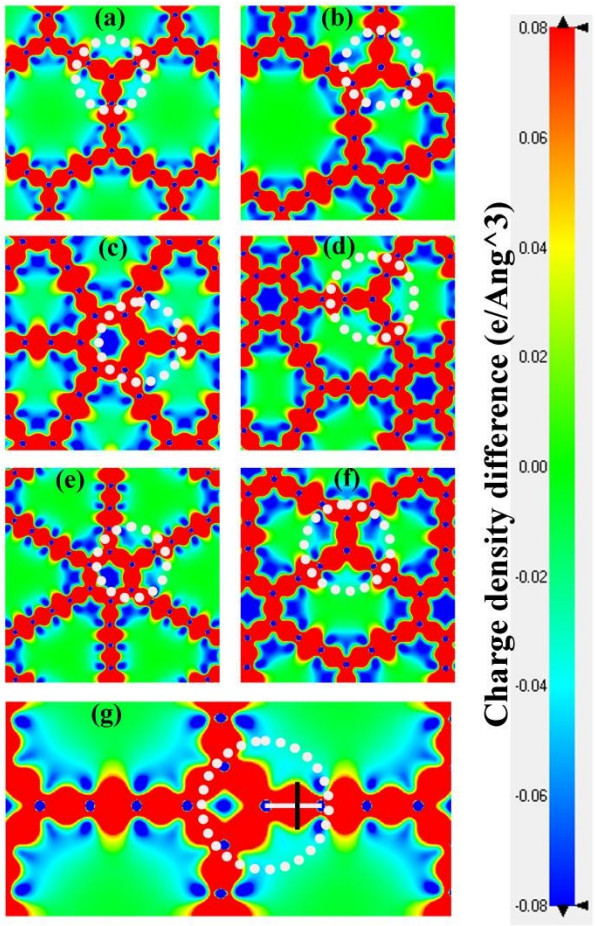

Figure 6.

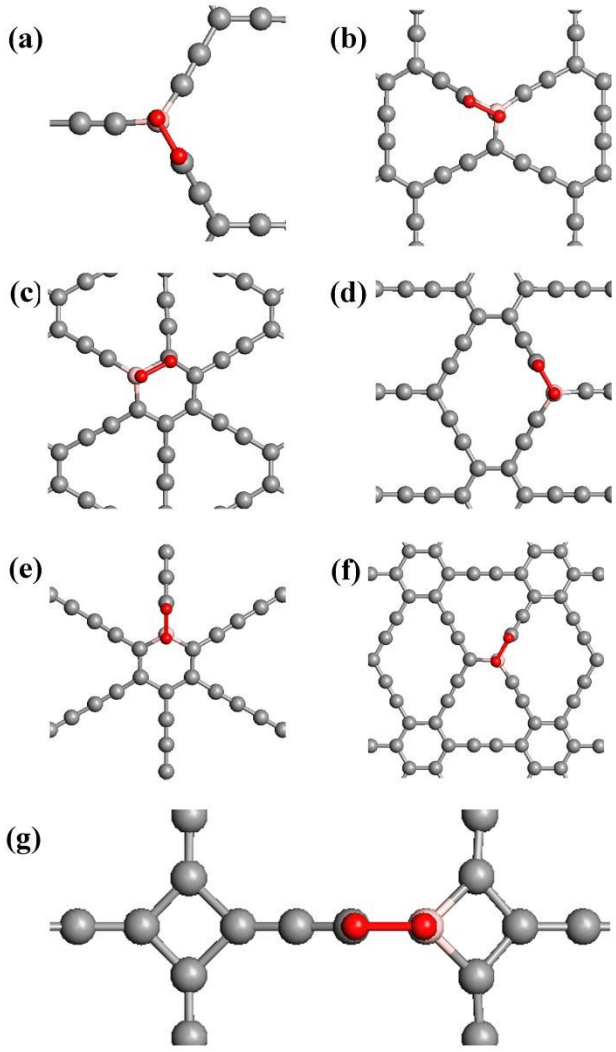

Figure 7.

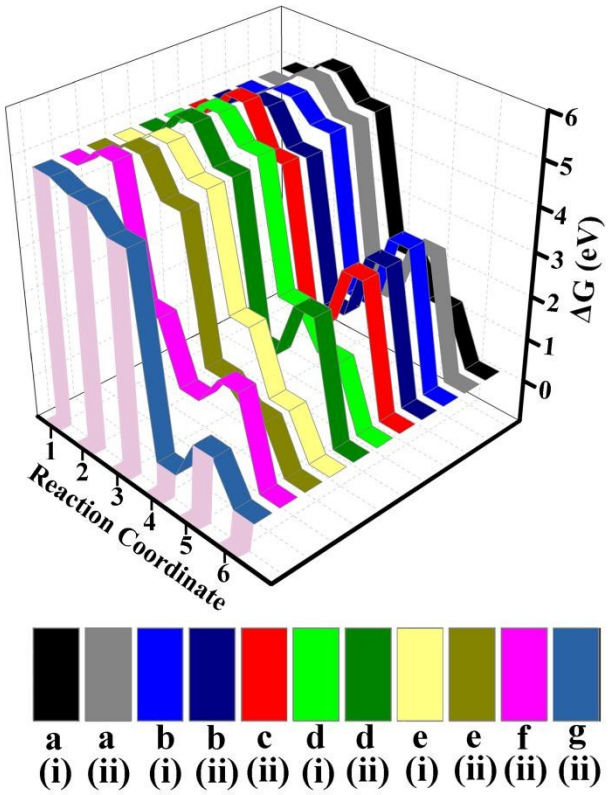

Figure 8.

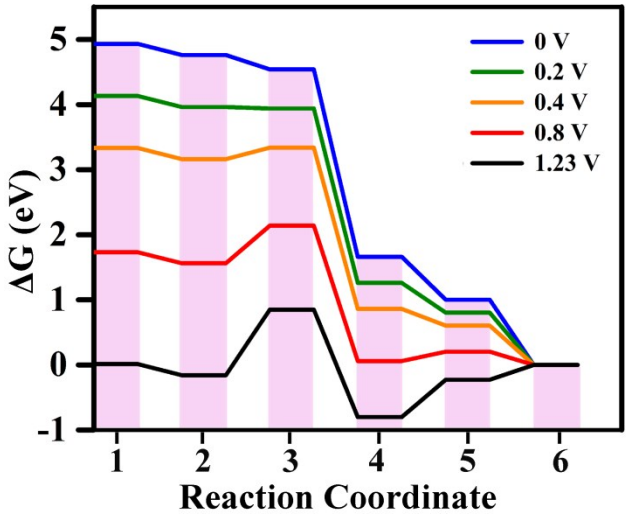

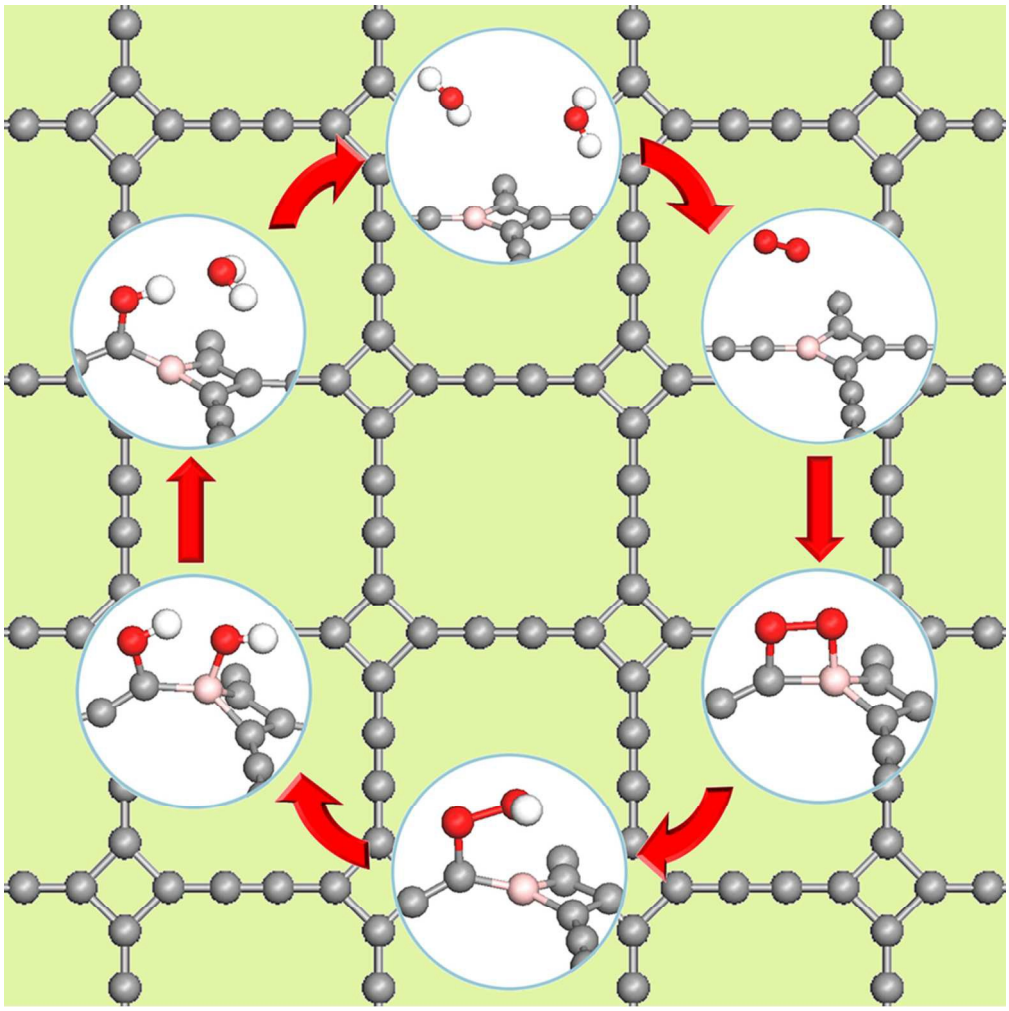

40x40mm (600 x 600 DPI)